

Piezospectroscopic measurement of high-frequency vibrations in a pulse-tube cryostat

Anne Louchet-Chauvet,¹ Rose Ahlefeldt,² and Thierry Chanelière^{1, 3, a)}

¹⁾*Laboratoire Aimé Cotton, CNRS, Univ. Paris-Sud, ENS-Cachan, Université Paris-Saclay, 91405, Orsay, France*

²⁾*Centre for Quantum Computation and Communication Technology, Research School of Physics and Engineering, The Australian National University, Canberra 0200, Australia*

³⁾*Univ. Grenoble Alpes, CNRS, Grenoble INP, Institut Néel, 38000 Grenoble, France*

(Dated: 22 January 2023)

Vibrations in cryocoolers are a recurrent concern to the end user. They appear in different parts of the acoustic spectrum depending on the refrigerator type, Gifford McMahon or pulse-tube, and with a variable coupling strength to the physical system under interest. Here, we use the piezospectroscopic effect in rare-earth crystals at low temperature as a high resolution, contact-less probe for the vibrations. With this optical spectroscopic technique, we obtain and analyze the vibration spectrum up to 700kHz of a 2kW pulse-tube cooler.

^{a)}Electronic mail: thierry.chaneliere@neel.cnrs.fr

I. INTRODUCTION

Compared to liquid helium cryostats, cryocoolers open many perspectives in the scientific community. First, closed-cycled systems allow to access cryogenic temperatures even when liquid helium is not available on-site. They can also be operated continuously with very limited maintenance, which is mandatory in many integrated applications or when remote control is required¹. The price to pay is a higher level of vibration for the cryocoolers compared to their *wet* equivalents². The measurement³ and the reduction of the vibrations in a cryocooler are active subjects of research, finding applications in very different fields including metrology for gravitational wave detection⁴, the definition of high stability oscillators⁵, or as a routine instrument for fundamental research^{6–11}.

These prospects have motivated many studies to accurately measure the vibration spectrum^{6,12} and to model it¹³ up to few tens of kHz. The noise is essentially dominated by the low-frequency components driven by the compression cycle. Higher frequencies are also present because of high-order harmonics of the tubes' mechanical distortion modes and smaller parts of the apparatus with higher resonant frequencies. The high frequency region of the spectrum may have an impact on micro or nano-mechanical resonators investigated at low temperatures to explore the quantum mechanical nature of massive objects¹⁴ or cryogenic mirrors for gravitational wave observation⁴, since both could have resonances falling into the high frequency range.

More fundamentally, proper modeling requires to measure a large spectrum in order to design accordingly a passive stabilization scheme. Active stabilization offers an alternative and elegant solution^{6,15}. This technique also requires the largest acquisition bandwidth to obtain a fast and reliable servo-control.

Accelerometers represent a commercial solution for measuring vibrations that are already compatible with cryogenic temperatures. They are routinely used to produce technical reports and allow a rapid comparison between different mechanical assembly of cryocoolers. When higher measurement bandwidths are targeted, optical techniques are particularly interesting. Fast response is guaranteed by current opto-electronics components, but they also offer a fine spatial resolution given by the beam size and an intrinsic nondestructive, contact-less character. Optical measurements are of two types: interferometric, when the surface under study reflects light as the end mirror of a Michelson interferometer, for example^{12,16}, or intensity sensor, usually based on fiber-coupled excitation and detection ports⁶. Both give access to the kHz frequency range, up to

20kHz¹², at least an order of magnitude better than most accelerometers. The detection bandwidth of optical techniques could also be pushed to higher frequencies, away from the audible spectrum, which have been mostly unexplored despite the absence of clear technical limitations.

We propose a new non-interferometric optical approach based on the piezospectroscopic effect in rare-earth doped oxide crystals at low temperature. The technique has the same advantages as other optical measurements: high bandwidth and no electrical contact on the sample, this latter representing a possible source of thermal and mechanical perturbations. The laser beam probes the stress induced by vibrations in the crystal instead of the change in distance between two reference points (as in, for example, interferometers). Piezospectroscopy has been used as a diagnostic tool for sapphire-based materials in which the inclusion of chromium can be used directly as a photoluminescent stress probe¹⁷. This *in-situ* method is particularly well-adapted to extreme fabrication conditions, as in high temperature reactors^{18,19}. It was also proposed in diamond NV-centers as a tool to detect the damage trail left by a weakly interacting massive particles (WIMPs)²⁰. Piezospectroscopy is even more relevant at low temperatures because atomic optical transitions become narrower, giving an enhanced sensitivity. This transition narrowing can be enhanced in rare-earth doped solids with the spectral-hole burning (SHB) mechanism, whose spectral resolution is in the MHz range²¹, well below the already narrow inhomogeneous linewidth at cryogenic temperature²² (chap.4).

Here, we use the piezospectroscopic effect in rare-earth doped oxides as a diagnostic tool, but it was initially identified as a strong limitation to high resolution measurements based on SHB performed using cryocoolers. In recent years, interest has arisen in using SHB for optical signal processing applications, such as RF spectral analysis^{23,24}, acousto-optic filtering²⁵, quantum memories²⁶, quantum opto-mechanics²⁷ and the definition of optical frequency standards²⁸. Thus, there is a strong need for cryogenic coolers with low vibrations for these different applications. Custom solutions have been used to reduce the vibrations to a level compatible with the targeted spectral resolution^{29–31}.

Beyond presenting a new technique for measuring vibrations in cryocoolers, our goal is to give a comprehensive analysis of the coupling between the vibrations and the rare-earth optical transition for the community studying these materials for signal processing applications. Our method could also establish a common testbed for different cryocoolers in order to compare the designs, upgraded or not, with custom isolation stages.

We first review the physics of piezospectroscopic measurements in rare-earth crystals. These

measurements were an active subject of research in the early days of laser spectroscopy, when they were used to identify the local site symmetry of dopant impurity in solids under static pressure. We extend the static case to SHB materials, more specifically $\text{Tm}^{3+}:\text{YAG}$ (yttrium aluminium garnet), under dynamical pressure fluctuations (vibrations). We then introduce and use our piezospectroscopic method to characterize the vibration of a pulse-tube cryocooler. We obtain and analyze a vibration spectrum up to 700kHz and partially correlate our measurement with the direct acoustic recording of the rotary valve.

II. PIEZOSPECTROSCOPY OF RARE-EARTH CRYSTALS

The piezospectroscopic effect of rare-earth luminescent transitions was investigated in the 60's following the seminal work of Kaplyanskii^{32,33}. Under applied pressure, rare earth levels shift and split, and this information can be used to determine the local site symmetry and thus understand how the dopant rare-earth ion is included within the crystalline cell. The intrinsically narrow line of optical 4f-4f transitions makes the measurement of shifts and splittings possible even at room temperature, if a diamond anvil cell is used to apply tens of GPa.

We first briefly review static pressure measurements that involved different lanthanide dopants in oxide and fluoride crystals, commonly fabricated and used for lasers. We perform the same static measurement by employing the highly sensitive SHB technique in $\text{Tm}^{3+}:\text{YAG}$ giving access to much higher resolution and much lower applied pressure. We finally discuss the correspondence between the dynamical pressure fluctuations, namely the vibrations, and the static measurements.

A. Static pressure measurements

The application of a static pressure allows one to extract information about the local crystal field surrounding the luminescent center. We briefly and partially review a few results of piezospectroscopic measurements in rare-earth doped oxides and fluorides (see Table I).

A wide range of dopants, transitions and host matrices has been studied in the references³⁴⁻⁴⁰, and in Table I we give some representative values. Despite very different combinations of transitions and crystals, the piezospectroscopic coefficients (in Hz/Pa) have very similar values and are dispersed by less than an order of magnitude. This similarity is related to the structural resemblance of the crystals. The piezospectroscopic effect is an indirect Stark shift induced by a mod-

Refs	Ion ³⁺	Transition	Crystal	Shift (Hz/Pa)
³⁴ (Table III)	Pr	$^3H_4 \rightarrow \text{avg.}$	LaOCl	-242.92
³⁵ (Table I)	Nd	$^4F_{3/2}(1) \rightarrow ^4I_{9/2}(1)$	YLiF ₄	-37
³⁶ (Table 1)	Pr	$^3H_4(1) \rightarrow ^1D_2(1)$	YLiF ₄	-172
³⁷ (Table I)	Nd	$^4F_{3/2}(1) \rightarrow ^4I_{9/2}(1)$	YVO ₄	-193
³⁸ (fig.1)	Nd	$^4F_{3/2} \rightarrow ^4I_{9/2}$	LiNbO ₃	~ -270
³⁹ (fig.1a)	Pr	$^3H_4 \rightarrow ^1D_2$	YAG	~ -100
²⁸ (fig.3)	Eu	$^7F_0 \rightarrow ^5D_0$ (site 1)	Y ₂ SiO ₅	-211
²⁸ (fig.3)	Eu	$^7F_0 \rightarrow ^5D_0$ (site 2)	Y ₂ SiO ₅	-52
⁴⁰ (fig.7a)	Yb	$^2F_{7/2}(1) \rightarrow ^2F_{5/2}(1)$	GGG	76

TABLE I: Review of piezospectroscopic measurements in rare-earth crystals. GGG stands for gadolinium gallium garnet. $^4F_{3/2}(1)$ means, for example, the first (lowest) crystal field level of the $^4F_{3/2}$ multiplet. Site 1 or 2 are two crystallographic sites of Y₂SiO₅²⁸.

ification of the crystalline electric field surrounding the rare-earth dopant. The applied pressure translates into a compression (strain) which brings the ionic charges closer. The dopant transitions are then shifted due to their sensitivity to electric fields (the Stark effect). The linear Stark shift in rare earth 4f-4f transitions varies only by about two orders of magnitude across different ions and host materials⁴¹ (Table 2). The variation in Young's modulus and inter-atomic distances is even smaller, resulting in comparable Stark coefficients across very different materials.

Meanwhile, lanthanide inter-shell 4f-5d transitions have much stronger piezospectroscopic coefficients, as for example 4200 Hz/Pa for Pr³⁺ in YAG⁴². The reason is that the 4f orbitals of the lanthanides are inner shells benefiting from a lower sensitivity to environmental changes, including the piezospectroscopic effect. In terms of measurement technique, the lower sensitivity of the intra-shell 4f-4f transitions is nevertheless largely compensated by the much narrower linewidth when probed by narrowband lasers. The resolution is, in that case, not limited by the inhomogeneous broadening (few GHz), but the homogeneous linewidth (below MHz) when the SHB technique is used, as we will see in section II B.

In summary, a typical value of 100 Hz/Pa can be kept in mind to evaluate the order of magnitude of pressure-induced shifts. As we will see now, the ${}^3H_6 \rightarrow {}^3H_4$ transition of $\text{Tm}^{3+}:\text{YAG}$ at our wavelength of interest (793nm) falls in this range as well.

B. Piezospectroscopy of $\text{Tm}^{3+}:\text{YAG}$

The SHB technique has been extensively used to measure the homogeneous linewidth of many rare-earth transitions and has been described in many textbooks, see²² (chap.4) for example. Put simply, the technique involves using a narrow band laser to select out a spectrally narrow portion of a broader atomic line by pumping atoms into a non-resonant shelving state. The width of this artificially narrow line (the spectral hole) is determined by the linewidth of the laser, well below MHz for narrowband lasers (such as extended cavity diode lasers). For very narrow lasers, the resolution is eventually limited to a few kHz, the homogeneous broadening of rare-earth transitions such as those in $\text{Tm}^{3+}:\text{YAG}$. The lifetime of the spectral hole can be extremely long, hours or days, by applying a field and shelving population in the Zeeman hyperfine structure^{43,44}. The SHB technique has been refined to the extreme in the context of optical metrology^{28,31} and used to accurately measure the detrimental shifts induced by the environmental changes, including pressure shifts³⁰.

In Fig.1, we show the effect of a small applied pressure on the shape and position of a spectral hole on the ${}^3H_6 \rightarrow {}^3H_4$ transition of $\text{Tm}^{3+}:\text{YAG}$. The initial hole (without pressure) is 50 kHz broad, significantly larger than the homogeneous linewidth ($\sim 3\text{kHz}$) because of power broadening. This resolution is sufficient to observe the dramatic effect of even a few kPa.

A splitting of the line is actually expected when a pressure is applied along the [110] crystal axis in YAG^{32,33}. Tm substitutes for Y in the YAG cell at a site of D_2 symmetry. This site has 6 possible orientations relative to the crystallographic axes, numbered from 1 to 6 (Ref. 45, Fig. 1 and references therein). Five of these sites contribute to the spectral hole in Fig. 1, site 1, and sites 3 to 6. Site 2 does not, because the optical transition is polarized, and for site 2 this polarization is parallel to the beam propagation direction, so the site is not excited. For pressure along [110], sites 3 to 6 are equivalent, and shift as a group in one direction, while site 1 shifts in the other, resulting in the split line in Fig. 1. Which peak corresponds to which site was determined by looking at the polarisation dependence of the split peaks.

The goal of our paper is not to describe extensively the piezospectroscopy effect in $\text{Tm}^{3+}:\text{YAG}$,

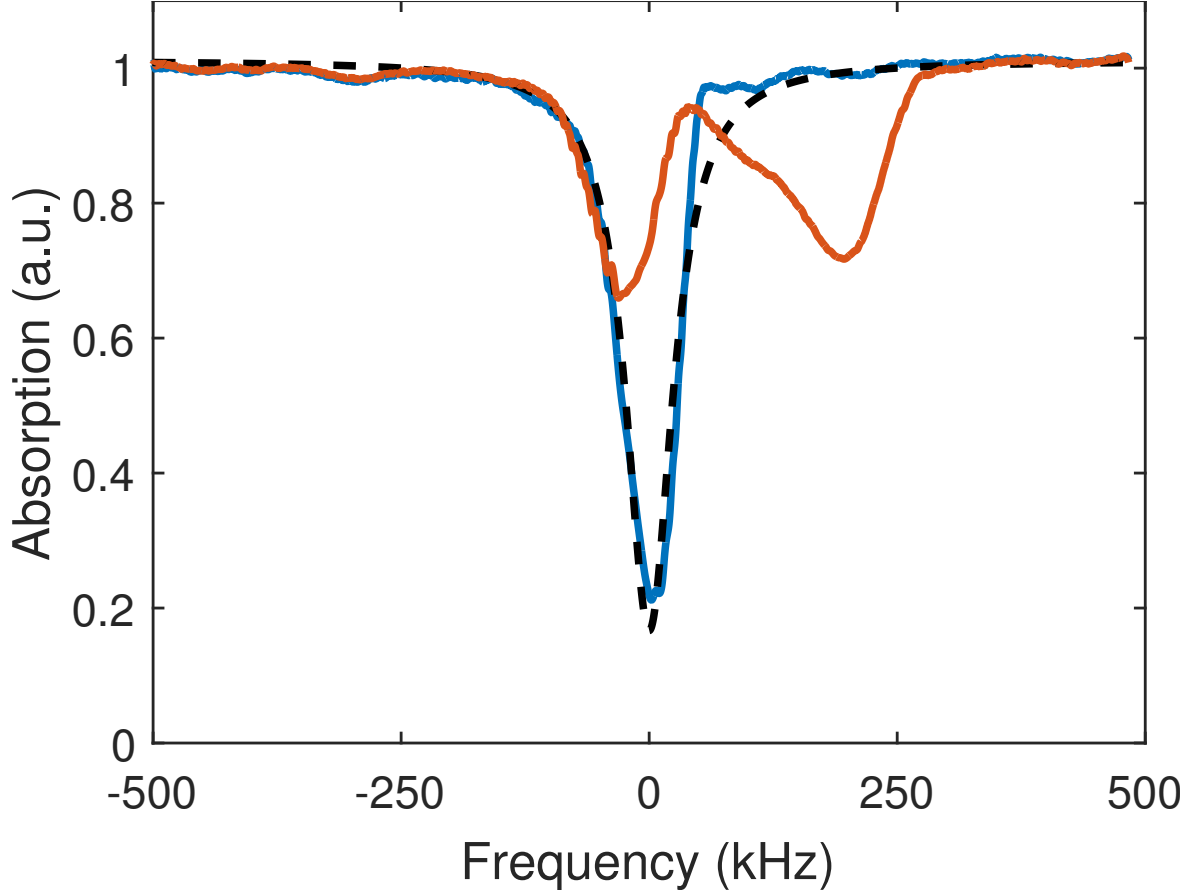


FIG. 1: Example of SHB absorption spectrum in $\text{Tm}^{3+}:\text{YAG}$ (blue line). The hole has a roughly Lorentzian shape (black dashed line) of 50kHz width (FWHM). When a 3.3kPa pressure is applied along the [110] crystal axis, the line splits in two components (red line) that shift (and broaden) independently (see text for details).

but rather to give a general idea of the link between the pressure vibrations and the optical transition. The measurement in Fig. 1 is illustrative and gives an order of magnitude of the pressure shifts. It was obtained in a dedicated variable temperature insert (VTI) cryostat (2-3K) that was used to apply a calibrated pressure and perform the piezospectroscopic analysis of our $\text{Tm}^{3+}:\text{YAG}$ sample. The shift in Fig. 1 was measured as a function of the applied pressure. To vary the pressure, we used a piezoelectric actuator (Thorlabs AE0203D04F) that was inserted in the cryostat and constrained in contact with the crystal. To calibrate the piezo response, which is unknown at low temperature, we applied a static pressure by loading, with a calibrated weight, an inner rod that presses on the crystal through the VTI sample holder. A few volts across the piezo corresponds to 10 kPa (a few tens of grams on the crystal surface).

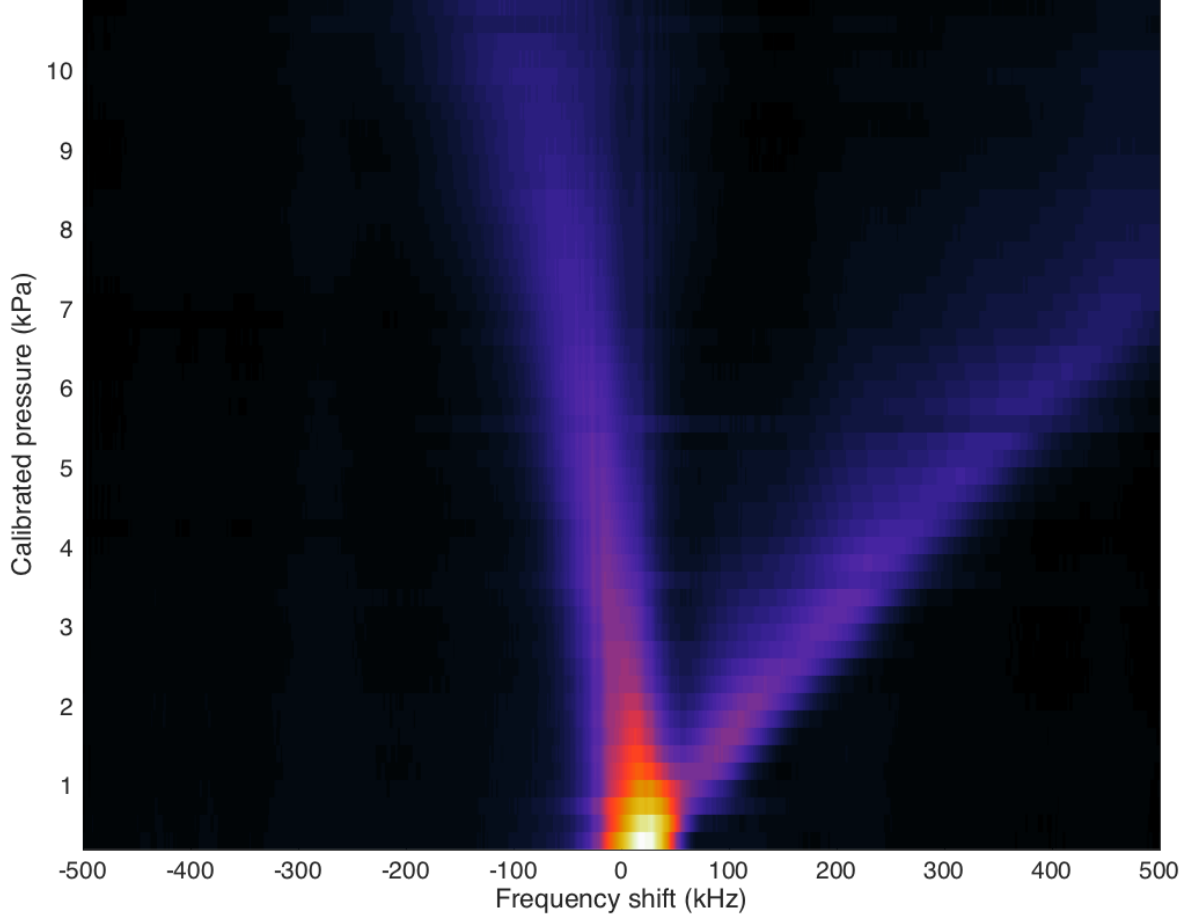


FIG. 2: Pressure shifts of the different crystallographic sites when the pressure is applied along [110]. The laser polarisation is along [110] as well, and so addresses only sites 1 and 3 to 6. Site 1 causes the peak with large positive shift 68 Hz/Pa, and sites 3 to 6 the peak with a small negative shift -13 Hz/Pa.

We can see in Fig. 2 that the lines split with different pressure coefficients for the different crystallographic sites. The splittings as a function of the piezo calibrated voltage are linear and allow us to extract a 68 Hz/Pa coefficient for site 1 and -13 Hz/Pa to sites 3, 4, 5 and 6. A complete analysis of the piezospectroscopic tensor for the different sites is beyond the scope of the paper. We will keep the value of 68 Hz/Pa as reference. We first see that $\text{Tm}^{3+}:\text{YAG}$ has a similar shift to other rare earth materials (see Table I). We note that the line showed substantial broadening as well as splitting, indicating that not all ions in the crystal experienced the same pressure. This shows that it is difficult, even in a well-controlled measurement, to apply a uniaxial pressure that only shifts and does not broaden the line. In addition, the presence of multiple site orientations means that an applied pressure would shift all the sites differently. Combined, these

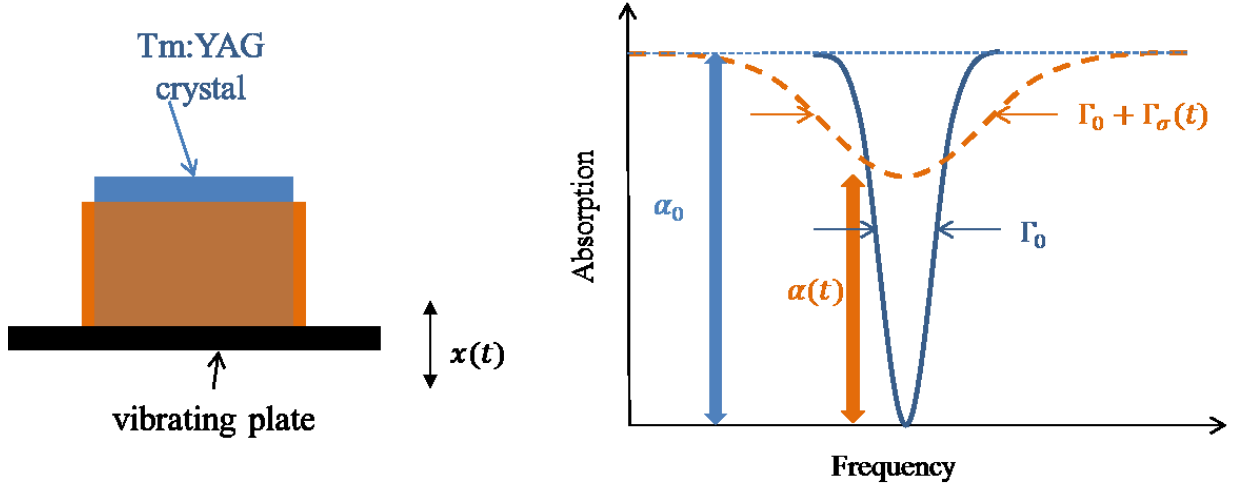


FIG. 3: Toy model relating the vibrations and the piezospectroscopic measurement. Left: the vibrating plate (along x) induces a compression of the crystal (unconstrained in blue and compressed crystal in orange). Right: We assume that the compression broadens the spectral hole (from the solid blue to the dashed orange curve) and therefore reduces the hole size and increases the measured absorption in the center of the hole due to hole area conservation.

two features mean that the vibrations in a cryocooler are most likely to broaden the spectral line, with the amount of broadening a measure of the local strain in the crystal. Thus, we will use the measured piezospectroscopic coefficient $\kappa = 68 \text{ Hz/Pa}$ as representative of the line broadening in $\text{Tm}^{3+}:\text{YAG}$.

C. Piezospectroscopy and vibrations

Above we described the physical origin of the piezospectroscopic effect and illustrated the discussion with a static pressure measurement in $\text{Tm}^{3+}:\text{YAG}$. The extension of this work to the case of vibrations, as dynamical pressure fluctuations, is not direct and requires some modeling. We propose a toy model in which the sample is attached to a vertically vibrating plate (see fig. 3)

The piezospectroscopic effect is due to the compression of the crystal when pressure is applied. This latter is related to the strain by $\sigma = E\Delta L/L$ where E is the Young's modulus and $\frac{\Delta L}{L}$ the relative compression (L is the sample length along x). In our model, the crystal is attached at one end where the vibration are induced as $x(t)$. For a unidirectional propagation of the vibration, the compression is due to the retarded propagation of sound in the material, so quantitatively,

$\Delta L = x(t) - x(t - L/V)$ where V is the sound velocity in the solid. For acoustic waves below 1 MHz, the wavelength is much longer than the crystal so we can write $\frac{\Delta L}{L} = \frac{\dot{x}(t)}{V}$ or for the strain $\sigma = \frac{E}{V}\dot{x}(t)$ to the first order.

The relation between the strain induced in the sample and the atomic line shape is not trivial. As we discussed in II B, a uniaxial pressure should in principle split the different sites. As we have seen, obtaining a pure shift without broadening is quite challenging in the static case because of the effective inhomogeneity of the strain field in the crystal along the axis of the laser. In the dynamical case, we expect the strain field to be even less homogeneous so the line is essentially broadened by the vibration, summing the effect of ions in different locations in the crystal and of each crystallographic site. The line broadening $\Gamma_\sigma = \kappa|\sigma|$ can then be related to the crystal velocity:

$$\Gamma_\sigma^{\text{[Hz]}}(t) = \kappa \frac{E}{V} |\dot{x}(t)| = 2.5 \times 10^9 |\dot{x}^{\text{[m/s]}}(t)| \quad (1)$$

where the numerical example corresponds to YAG with $E = 300$ GPa and $V = 8165$ m/s. The value of $\kappa = 68$ Hz/Pa is inferred from the spectral hole shift measurements reported in section II B.

The absolute value of the velocity in Eq. 1 makes it mathematically impossible to determine the signed velocity. To proceed with the calculation we are compelled to removing the absolute value, which comes down to assuming that negative strain leads to a narrowing of the spectral hole or that there is no negative strain at all. We expect this simplification to distort the sample displacement spectral density, with a possible doubling of the dominating frequencies, and the appearance of high frequency artefacts in the case of sharp features close to zero. The displacement spectral density will therefore be analyzed with caution.

The linewidth broadening induced by the vibration can be estimated optically by probing the absorption at the center of the hole as sketched in Fig. 3 (right) and as will be discussed in more details in IV A. A line broadening (for example by a factor of 3 in Fig. 3, right) increases the absorption in the center of the spectral hole accordingly.

We can write the hole linewidth in terms of the measured absorption at the center of the spectral hole, and the original spectral hole width without vibrations Γ_0 . The vibration makes the hole width increase up to $\Gamma_0 + \Gamma_\sigma(t)$, leading to a varying absorption coefficient $0 \leq \alpha(t) \leq \alpha_0$ where α_0 is the absorption in the absence of the spectral hole. Assuming a spectral hole broadening as previously discussed, and the conservation of the hole area, we write:

$$[\alpha_0 - \alpha(t)][\Gamma_0 + \Gamma_\sigma(t)] = \alpha_0 \Gamma_0 \quad (2)$$

leading to :

$$\Gamma_{\sigma}(t) = \frac{\alpha(t)}{\alpha_0 - \alpha(t)} \Gamma_0 \quad (3)$$

This simply reflects the conservation of the absorbing centers involved in the SHB process, which is valid as long as the hole is measured over times shorter than the hole decay time.

As a conclusion, by using a simple model, we can relate the vibration (Eq.1) to the time-resolved SHB spectroscopy of $\alpha(t)$ (Eq.2) and finally extract quantitatively the characteristic vibration through its velocity $\dot{x}(t)$.

III. MEASUREMENT SETUP

We used a pulse-tube cryocooler (TransMIT PTD-009) with an Oerlikon COOLPAK 2000A compressor. The rotary valve is rigidly attached to the cold head and has a cycle rate of 2 Hz. A sound level meter (RadioShack 33-099) was positioned in contact with the outer shield of the rotary valve and records the audio signal in the 1Hz–20kHz range.

A copper inner vacuum chamber is attached to the second stage at 2.9 K. It will be used for further isolation with exchange gas injection in the future but can simply be considered as a rigid sample mount for this experiment. The $\text{Tm}^{3+}:\text{YAG}$ sample was resting at the bottom of the chamber, thermally and rigidly contacted by Apiezon-N grease. The crystal was fabricated by Scientific Materials and is anti-reflection-coated on both sides to reduce interferometric effects. The laser propagated along the $[1\bar{1}0]$ crystallographic axis. The thulium concentration in the sample is 0.25 at.% so that the total absorption is $\alpha L \simeq 2$ for $L = 5$ mm. Further details about SHB in $\text{Tm}^{3+}:\text{YAG}$ including the population dynamics under optical excitation can be found in⁴⁶ (and references therein).

The narrow-band laser source was an extended cavity diode laser stabilized to a Fabry-Perot cavity via a Pound-Drever-Hall feedback loop and tuned close to the center of the $\text{Tm}^{3+}:\text{YAG}$ ${}^3H_6(1) \rightarrow {}^3H_4(1)$ absorption line (12604.42 cm^{-1}). The laser beam was spectrally and temporally shaped with an acousto-optic modulator (AA-Optoelectronics MT110) driven with an arbitrary waveform generator (Tektronix AWG5004). The $60 \mu\text{W}$ beam was focused into the sample with a $100 \mu\text{m}$ waist, corresponding to a Rabi angular frequency around 100 krad.s^{-1} . We detected the transmitted light through the crystal with an avalanche photodiode (Thorlabs APD110A). The photodiode and the soundmeter signals were acquired via a digital oscilloscope (Agilent DSO5034A) as a 2 s long trace containing 4 million points per channel, leading to a 2 MHz sampling frequency.

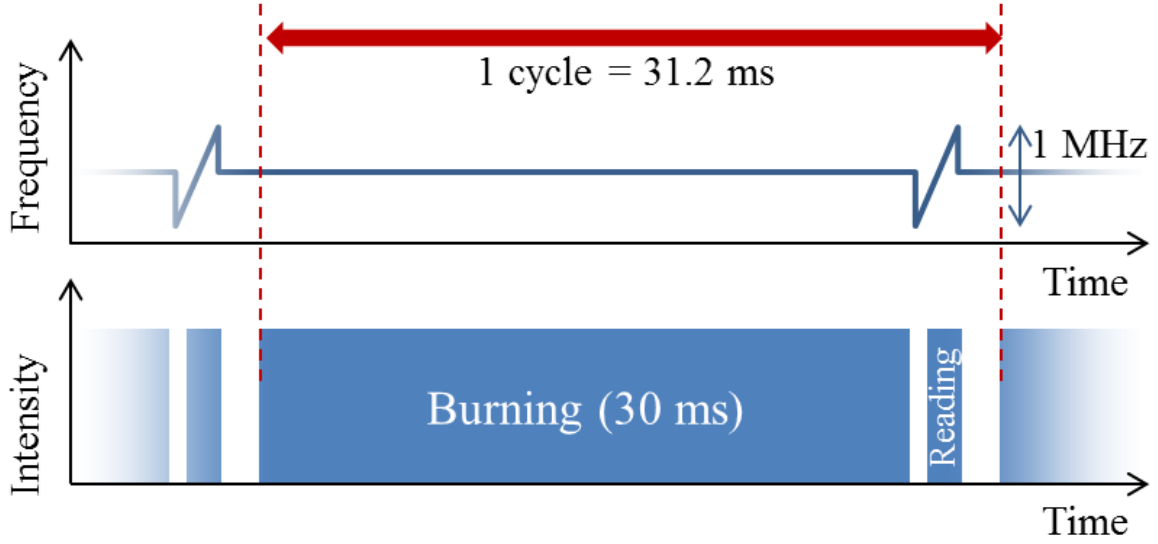


FIG. 4: Excitation pulse sequence. The burning pulse is monochromatic and lasts 30 ms, whereas the reading pulse is frequency chirped over 1 MHz in 200 μ s. Both pulses have the same power.

In an experiment, the hole amplitude at line center can be directly measured by monitoring the absorption of a laser burning a continuous spectral hole. A continuous measurement like this allows us to measure up to very high frequencies, limited only by the timing resolution of the acquisition system. However, it is still necessary to measure Γ_0 , the original width of the spectral hole, by chirping the laser over the hole to measure the hole shape. In the continuous scheme, this reading chirp must be done periodically, at an interval of 31.2 ms in our case, comparable to the lifetime of the spectral hole, to provide an accurate reference.

The periodic pulse sequence depicted in Fig. 4 was repeated with a 31.2 ms cycle time, *ie* around 16 times per rotary valve cycle. The 30 ms burning pulse filled 96% of the cycle time and can therefore be regarded as almost continuous. The hole decay time was typically 10 ms (limited by the lifetime of the Tm metastable state 3F_4) so each burning-reading step can be considered as independent. The 100 μ s reading pulse was linearly chirped around the burning frequency so as to provide a measurement of the hole shape.

We first plot the hole shape, measured by the reading chirped pulse, throughout 3 rotary valve cycles together with the audio level in Fig. 5. The FWHM of the spectral hole oscillates between 150 kHz and 350 kHz depending on the position of the scan in the rotary valve cycle. This broadening is the result of the 30 ms burning pulse under vibration. More specifically, the spectral

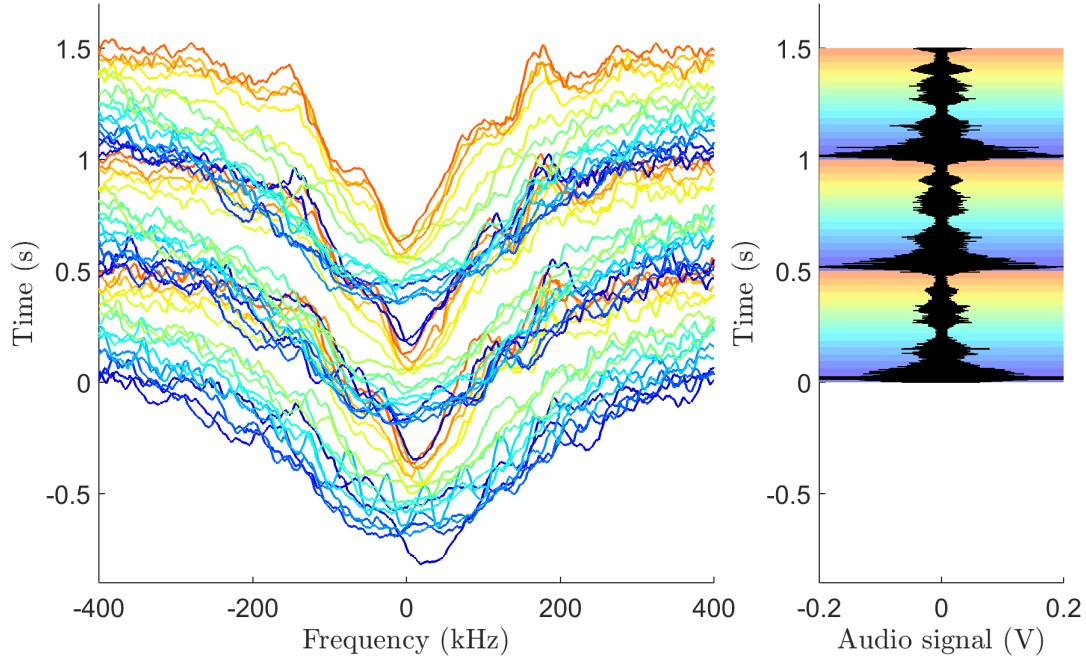


FIG. 5: Left: Spectral hole absorption throughout 3 rotary valve cycles (*ie* 48 sequence cycles). The graphs are vertically offset for a clear view of the spectral hole evolution with time. Right: the audio signal is simultaneously recorded (black line). Each sequence cycle is identified with a color (from blue at the beginning of the rotary valve cycle to orange at the end).

hole is narrowest at the beginning of the cycle (that we define as the time where the sound level is maximum), then suddenly broadens after 60 ms, remains broad for around 0.3 s and then gets narrow again for the remaining 0.2 s of the rotary valve cycle.

IV. DATA ANALYSIS

A. Monitoring the vibration via the atomic absorption

The burning pulse both burns and probes the hole, providing a continuous readout of the hole amplitude. The read pulse periodically measures the entire hole shape, and is used as a reference for the hole width Γ_0 inferred from the amplitude measurement of the burn pulse. More precisely, according to Bouguer-Beer-Lambert's absorption law, the transmission signal collected on the avalanche photodiode during the burning pulse is proportional to $e^{-\alpha(t)L_0}$ (L_0 is the laser propagation distance), eventually yielding the hole instantaneous broadening $\Gamma_\sigma(t)$ due to the vi-

brations, using Eq. 3. The reference hole width Γ_0 is derived from the hole spectrum measured immediately after a given burning pulse in the repeated sequence of Fig. 4.

A typical example of the hole broadening $\Gamma_\sigma(t)$ and of the sound level $V_{ac}(t)$ measured simultaneously are given in Fig. 6. We observe that the hole broadening oscillates at frequencies above 20 kHz and its value often exceeds 100 kHz in the first 0.3 s of each rotary valve cycle. The spectral hole perturbations are slightly delayed with respect to the rotary valve cycle. The acoustic noise and the piezospectroscopic perturbation have a common origin and are both triggered at the same time in the compression cycle. However, there is no direct relation between the two spectra, indicating that the vibration in the sample is not directly correlated to the vibration frequencies of the rotary valve itself.

B. Spectro-temporal analysis

We calculate the single-sided amplitude spectral density⁴⁷ of the hole broadening for each sequence cycle:

$$A_{\Gamma_\sigma}(f) = \sqrt{\frac{2}{T}} |\tilde{\Gamma}_\sigma(f)|, \quad (4)$$

where $\tilde{\Gamma}_\sigma(f) = \int_{-T/2}^{T/2} \Gamma_\sigma(t) e^{2i\pi ft} dt$ is the Fourier transform of the hole broadening $\Gamma_\sigma(t)$ over the burning pulse duration $T = 30$ ms. $A_{\Gamma_\sigma}(f)$ is expressed in $\text{Hz}/\sqrt{\text{Hz}}$. We calculate the hole broadening spectral density for each sequence cycle, and plot the result in the form of a spectrogram in Fig. 7(a), averaged over 150 acquisitions.

In Eq. 1 we gave the link between the hole broadening and the sample velocity. As explained in section II B we drop the absolute value in the equation. Displacement and velocity are linked by a derivation operation in the time-domain, which translates into $\tilde{x}(f) = 2i\pi f \tilde{x}(f)$ in the spectral domain. We thus obtain the displacement spectral density:

$$A_x(f) = \frac{V}{\kappa E 2\pi f} A_{\Gamma_\sigma}(f) \quad (5)$$

that we display in Fig. 7(b). Finally, Fig. 7(c) shows the spectrogram of the audio signal spectral density $A_{V_{ac}}(f)$ measured on the rotary valve.

The audio spectrogram clearly shows the rotary valve cycles at 2 Hz, with the high-pitched chirp (around 10 kHz) that can be heard twice per valve cycle, in agreement with previously reported cryocooler audio spectrograms⁴⁸. From the hole broadening and displacement spectrograms, we can define two uneven alternating steps in the rotary valve cycle that were already visible in Fig. 6:

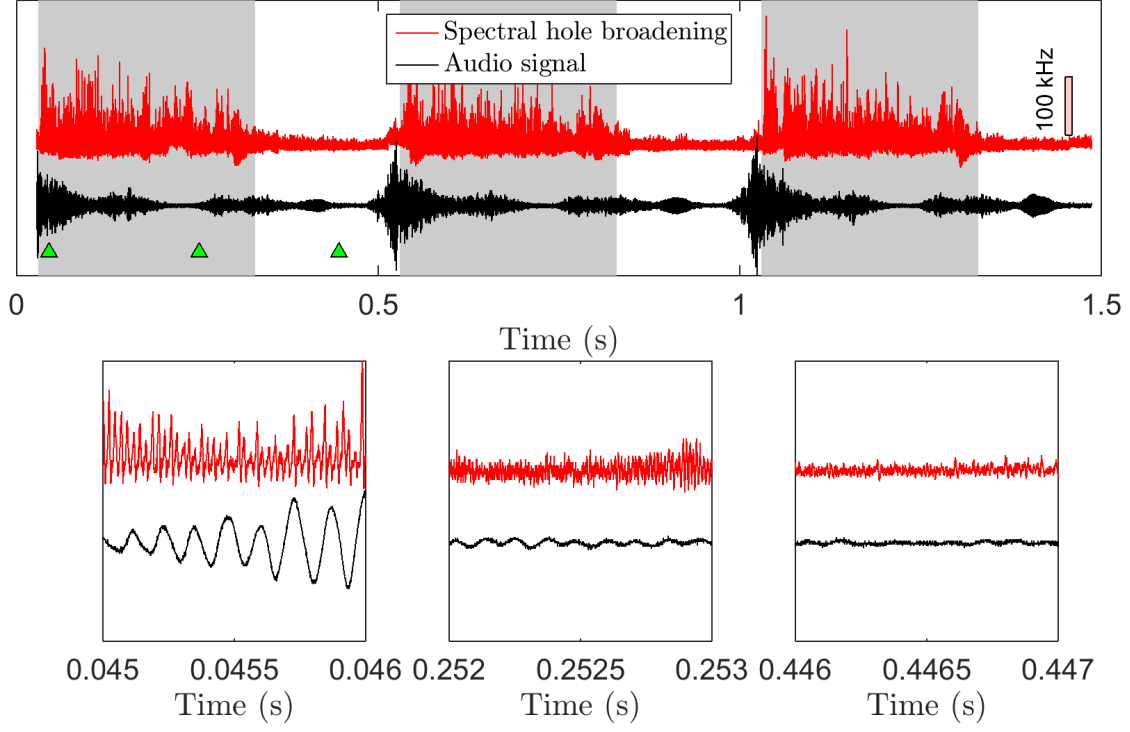


FIG. 6: Experimental traces of the sound level $V_{ac}(t)$ (black) and the spectral hole broadening $\Gamma_{\sigma}(t)$ (red) deduced from the absorption measurement through the spectral hole during the burning sequence. The rectangle on the right gives the scale for the hole broadening trace. The 0.3 s wide gray areas represent the so-called “noisy” phase defined in Sec. IV B. The three lower graphs show the same traces on a 1 ms interval at times indicated by a green triangle on the main graph, corresponding to different positions in the rotary valve cycle.

a noisier step, starting almost together with the loud rotary valve chirp and lasting 0.3 s, followed by a quieter step lasting 0.2 s. These two steps are not visible in the acoustic spectrogram, confirming that the vibration of the rotary valve is not transmitted to the cold finger in a straightforward manner.

C. Vibration spectra

In Fig. 8, we plot the displacement spectral density as a multiplot with the same color code as in Fig 5. At 1 kHz, $A_x(f)$ is equal to $2 \cdot 10^{-11} \text{ m}/\sqrt{\text{Hz}}$ in the noisy phase, and $2 \cdot 10^{-13} \text{ m}/\sqrt{\text{Hz}}$ in the quiet phase. This is two to three orders of magnitude lower than the values measured

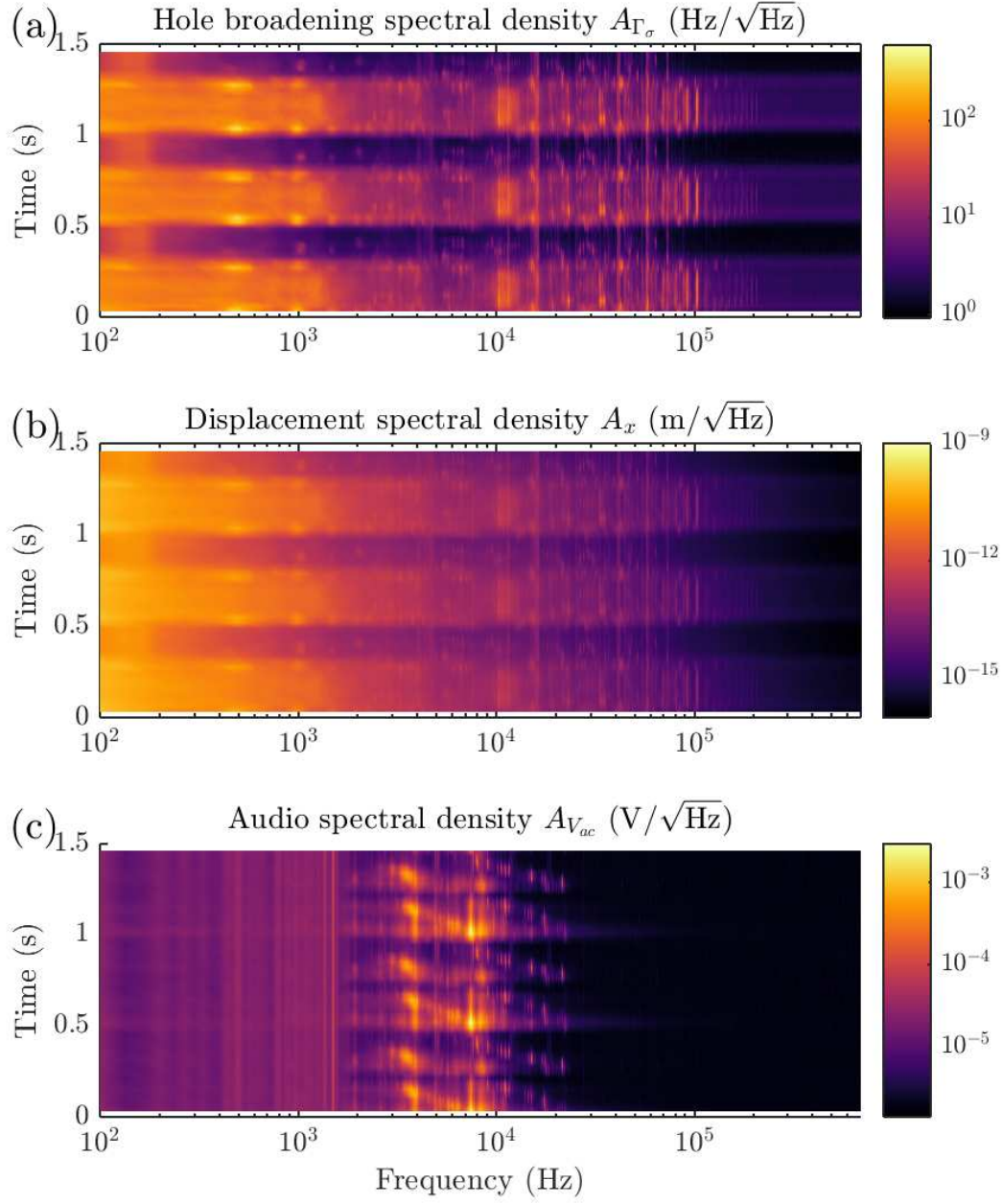


FIG. 7: Amplitude spectral density spectrograms of (a) the spectral hole broadening, (b) the corresponding displacement, and (c) the audio sound level on the rotary valve.

in other pulse-tube cryocoolers with no vibration isolation (between 10^{-8} m/ $\sqrt{\text{Hz}}$ with optical detection³ and $5 \cdot 10^{-10}$ m/ $\sqrt{\text{Hz}}$ with accelerometric detection¹⁵). This discrepancy could be explained by an inaccurate estimation of the displacement, or a lower vibration level of our low-

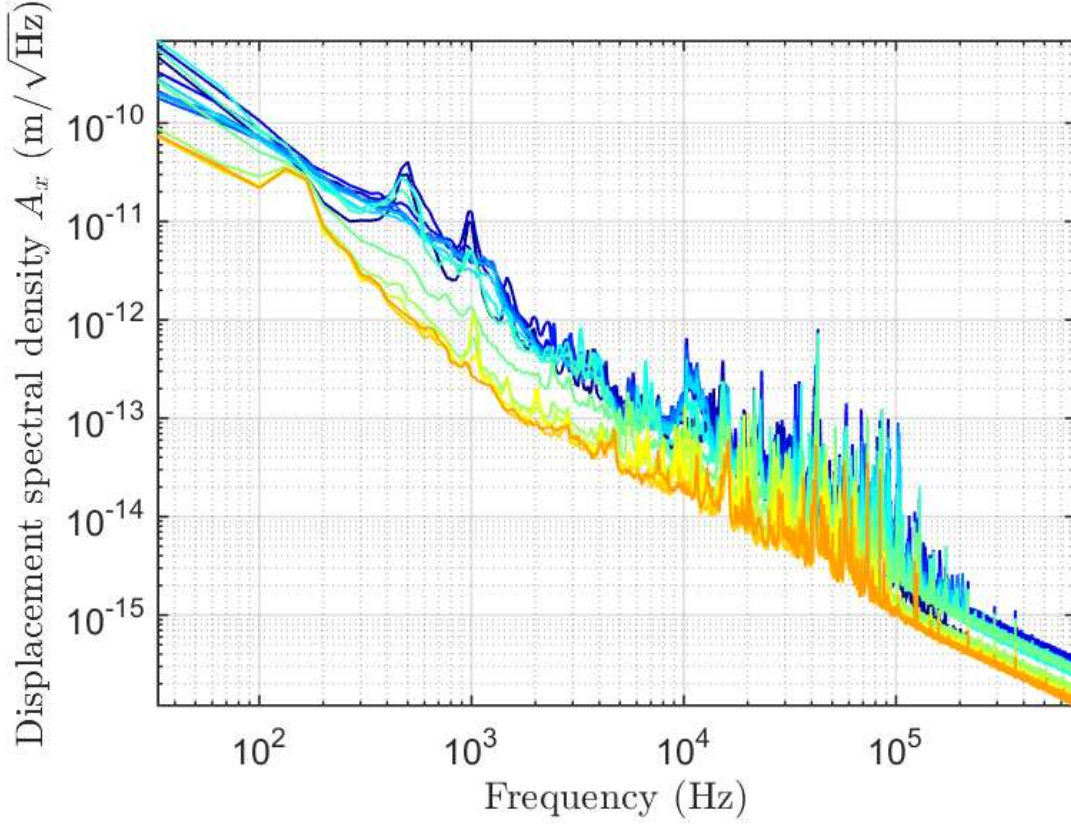


FIG. 8: Cold finger displacement spectral density derived from the absorption of a spectral hole in a Tm-doped crystal at 2.9 K. The lines are colored according to their position in the rotary valve cycle, from blue at the beginning to orange at the end.

power pulse-tube cooler compared to previously measured instruments. We discuss these in turn. There is an inaccuracy in the quantitative estimation of the vibration amplitude, because of the simplistic model used to relate the crystal absorption to the local strain, the somewhat empirical determination of the piezospectroscopic coefficient κ (by taking a typical averaged value of the measured shifts in II B), and the assumption of only positive strain.

It should be also noted that the originality of our method makes the comparison with other optical vibration measurements difficult. This is a general issue when comparing different cryocoolers characterized with different techniques. As an example, our pulse-tube has a low input power (2kW) as compared to other vibrations studies^{3,15} (typically 7kW). This makes direct comparisons generally challenging.

More fundamentally, the piezospectroscopic effect is sensitive to the local stress applied on the crystal attached to the second stage. Other optical methods intrinsically measure the relative

positive of the cold plate with respect to a reference point on the pulse-tube or the optical table base plane. There is a priori no good or bad method. The appropriateness depends on the measurement of interest driven by the application. Different techniques should be seen as complementary to give a more complete characterization of the vibrations. In that sense, our measurements could be more quantitative if connected at lower frequencies to another type of measurement (*ie* with 3-axis accelerometers).

Due to its intrinsic sensitivity to velocity, our method’s sensitivity to displacement increases with the frequency. It operates between 100 Hz and 1 MHz. The lower value is imposed by the spectral hole lifetime (10 ms for Tm:YAG²² (chap.7)), whereas the upper value is a purely technical limit since it corresponds to the Nyquist frequency, *ie* 1 MHz.

V. CONCLUSION

In this paper, we presented a novel optical method based on the piezospectroscopic effect in a rare-earth ion-doped crystal for the detection of high frequency (> 100 Hz) vibration in a cold environment. Although not fully quantitative, this method is multidirectional and contact-less. Its sensitivity increases with frequency and has no fundamental upper frequency limit.

For our demonstration, we used a cryocooler with optical windows. Nonetheless, further integration of the setup (primarily the crystal and the detector) is totally possible to form a compact sensor with a fibered input feed-through (probe laser) and electric readout port (photodetector output). This integration step would allow to characterize a much wider range of cryocoolers without optical access.

VI. ACKNOWLEDGMENTS

We are grateful to E. Olivieri and C. Marrache-Kikuchi for stimulating discussions. We thank also J. Paris (My Cryo Firm), J. Falter (TransMIT) and P. Pariset (CNRS-LAC) for technical assistance on the pulse-tube maintenance and design.

This work was supported by ITMO Cancer: AVIESAN (National Alliance for Life Sciences & Health) within the framework of the Cancer Plan, by the Investissements d’Avenir du LabEx PALM ExciMol and OptoRF-Er (ANR-10-LABX-0039-PALM), by the DIM Nano-K project RECTUS and by the CMDO+ network (Mission pour l’Interdisciplinarité du CNRS).

Appendix A: Discarding the Doppler effect

In this paper, we have identified the piezospectroscopic effect as the principal source of coupling between vibrations and the optical absorption. As we discussed, rare-earth transitions are quite sensitive to strain because of their exceptionally narrow linewidth. This atomic-like feature for a solid impurity may give the impression that the Doppler shift induced by the vibrations could be a source of perturbation. We take the opportunity to show that the Doppler shift or broadening is much weaker than the piezospectroscopic effect.

The Doppler effect that would induce a similar broadening that the one discussed in II C is also proportional to the crystal velocity. It is given by

$$\Gamma_D^{[\text{Hz}]}(t) = \frac{1}{\lambda} |\dot{x}(t)| = 1.3 \times 10^6 |\dot{x}^{[\text{m/s}]}(t)| \quad (\text{A1})$$

where $\lambda = 793 \text{ nm}$ is the transition wavelength for our crystal. A direct comparison with Eq.(1) is then possible. The Doppler effect is three orders of magnitude weaker than the piezospectroscopic shift and can be fully neglected in first approach.

REFERENCES

- ¹H. Oh, K. Lee, and M. Jo, “A passive launch and on-orbit vibration isolation system for the spaceborne cryocooler,” *Aerospace Science and Technology* **28**, 324–331 (2013).
- ²R. Radebaugh, “Cryocoolers: the state of the art and recent developments,” *Journal of Physics: Condensed Matter* **21**, 164219 (2009).
- ³T. Tomaru, T. Suzuki, T. Haruyama, T. Shintomi, A. Yamamoto, T. Koyama, and R. Li, “Vibration analysis of cryocoolers,” *Cryogenics* **44**, 309–317 (2004).
- ⁴T. Tomaru, T. Suzuki, T. Haruyama, T. Shintomi, N. Sato, A. Yamamoto, Y. Ikushima, R. Li, T. Akutsu, T. Uchiyama, and S. Miyoki, “Vibration-free pulse tube cryocooler system for gravitational wave detectors, part i: Vibration-reduction method and measurement,” in *Cryocoolers 13*, edited by R. G. Ross (Springer US, Boston, MA, 2005) pp. 695–702.
- ⁵S. Grop, P. Bourgeois, N. Bazin, Y. Kersalé, E. Rubiola, C. Langham, M. Oxborrow, D. Clapton, S. Walker, J. De Vicente, *et al.*, “ELISA: A cryocooled 10 GHz oscillator with 10^{-15} frequency stability,” *Review of Scientific Instruments* **81**, 025102 (2010).
- ⁶S. Caparrelli, E. Majorana, V. Moscatelli, E. Pascucci, M. Perciballi, P. Puppo, P. Rapagnani,

- and F. Ricci, “Vibration-free cryostat for low-noise applications of a pulse tube cryocooler,” *Review of Scientific Instruments* **77**, 095102 (2006).
- ⁷B. Evans, R. Down, J. Keeping, O. Kirichek, and Z. Bowden, “Cryogen-free low temperature sample environment for neutron scattering based on pulse tube refrigeration,” *Measurement Science and Technology* **19**, 034018 (2008).
- ⁸C. Wang and J. G. Hartnett, “A vibration free cryostat using pulse tube cryocooler,” *Cryogenics* **50**, 336–341 (2010).
- ⁹J. Hackley, D. Kislitsyn, D. Beaman, S. Ulrich, and G. Nazin, “High-stability cryogenic scanning tunneling microscope based on a closed-cycle cryostat,” *Review of Scientific Instruments* **85**, 103704 (2014).
- ¹⁰F. Quacquarelli, J. Puebla, T. Scheler, D. Andres, C. Bödefeld, B. Sipos, C. Dal Savio, A. Bauer, C. Pfeleiderer, A. Erb, *et al.*, “Scanning probe microscopy in an ultra-low vibration closed-cycle cryostat: Skyrmion lattice detection and tuning fork implementation,” *Microscopy Today* **23**, 12–17 (2015).
- ¹¹R. Maisonobe, J. Billard, M. De Jesus, A. Juillard, D. Misiak, E. Olivieri, S. Sayah, and L. Vagneron, “Vibration decoupling system for massive bolometers in dry cryostats,” *arXiv preprint arXiv:1803.03463* (2018).
- ¹²A. Chijioke and J. Lawall, “Vibration spectrum of a pulse-tube cryostat from 1 Hz to 20 kHz,” *Cryogenics* **50**, 266–270 (2010).
- ¹³S. Riabzev, A. Veprik, H. Vilenchik, and N. Pundak, “Vibration generation in a pulse tube refrigerator,” *Cryogenics* **49**, 1–6 (2009).
- ¹⁴K. Schwab and M. Roukes, “Putting mechanics into quantum mechanics,” *Physics Today* **58**, 36–42 (2005).
- ¹⁵E. Majorana, M. Perciballi, P. Puppo, P. Papagnani, and F. Ricci, “Vibration free cryostat for cooling suspended mirrors,” in *Journal of Physics: Conference Series*, Vol. 32 (IOP Publishing, 2006) p. 374.
- ¹⁶L. Mauritsen, D. Snow, A. Woidtke, M. Chase, and I. Henslee, “Low vibration, low thermal fluctuation system for pulse tube and gifford-mcmahon cryocoolers,” *Cryocoolers* **15**, 581–585 (2009).
- ¹⁷J. He and D. Clarke, “Determination of the piezospectroscopic coefficients for chromium-doped sapphire,” *Journal of the American Ceramic Society* **78**, 1347–1353 (1995).
- ¹⁸R. Christensen, D. Lipkin, D. R. Clarke, and K. Murphy, “Nondestructive evaluation of the oxi-

- dation stresses through thermal barrier coatings using Cr³⁺ piezospectroscopy,” *Applied Physics Letters* **69**, 3754–3756 (1996).
- ¹⁹K. Schlichting, K. Vaidyanathan, Y. Sohn, E. Jordan, M. Gell, and N. Padture, “Application of Cr³⁺ photoluminescence piezo-spectroscopy to plasma-sprayed thermal barrier coatings for residual stress measurement,” *Materials Science and Engineering: A* **291**, 68–77 (2000).
- ²⁰S. Rajendran, N. Zobrist, A. O. Sushkov, R. Walsworth, and M. Lukin, “A method for directional detection of dark matter using spectroscopy of crystal defects,” *Physical Review D* **96**, 035009 (2017).
- ²¹As an order of magnitude, 400 GHz corresponds to 1 nm in the near IR.
- ²²G. Liu and B. Jacquier, *Spectroscopic properties of rare earths in optical materials*, Vol. 83 (Springer Science & Business Media, 2006).
- ²³K. Merkel, R. K. Mohan, Z. Cole, T. Chang, A. Olson, and W. Babbitt, “Multi-gigahertz radar range processing of baseband and RF carrier modulated signals in Tm:YAG,” *Journal of Luminescence* **107**, 62–74 (2004).
- ²⁴G. Gorju, V. Crozatier, I. Lorg  r  , J.-L. Le Gou  t, and F. Bretenaker, “10-GHz bandwidth RF spectral analyzer with MHz resolution based on spectral hole burning in Tm³⁺:YAG,” *IEEE Photonics Technology Letters* **17**, 2385–2387 (2005).
- ²⁵Y. Li, H. Zhang, C. Kim, K. Wagner, P. Hemmer, and L. Wang, “Pulsed ultrasound-modulated optical tomography using spectral-hole burning as a narrowband spectral filter,” *Applied Physics Letters* **93**, 011111 (2008).
- ²⁶K. Heshami, D. England, P. Humphreys, P. Bustard, V. Acosta, J. Nunn, and B. Sussman, “Quantum memories: emerging applications and recent advances,” *Journal of Modern Optics* **63**, 2005–2028 (2016).
- ²⁷K. M  lmer, Y. Le Coq, and S. Seidelin, “Dispersive coupling between light and a rare-earth-ion-doped mechanical resonator,” *Phys. Rev. A* **94**, 053804 (2016).
- ²⁸M. Thorpe, L. Rippe, T. Fortier, M. Kirchner, and T. Rosenband, “Frequency stabilization to 6×10^{-16} via spectral-hole burning,” *Nature Photonics* **5**, 688 (2011).
- ²⁹Y. Chen, X. Fernandez-Gonzalvo, and J. Longdell, “Coupling erbium spins to a three-dimensional superconducting cavity at zero magnetic field,” *Physical Review B* **94**, 075117 (2016).
- ³⁰M. Thorpe, D. Leibrandt, and T. Rosenband, “Shifts of optical frequency references based on spectral-hole burning in Eu³⁺:Y₂SiO₅,” *New Journal of Physics* **15**, 033006 (2013).

- ³¹O. Gobron, K. Jung, N. Galland, K. Predehl, R. Le Targat, A. Ferrier, P. Goldner, S. Seidelin, and Y. Le Coq, “Dispersive heterodyne probing method for laser frequency stabilization based on spectral hole burning in rare-earth doped crystals,” *Optics Express* **25**, 15539–15548 (2017).
- ³²A. Kaplyanskii, “Noncubic centers in cubic crystals and their piezospectroscopic investigation,” *Optics and Spectroscopy* **16**, 329 (1964).
- ³³A. Kaplianskii and A. Przhevuskii, “Deformation splitting and the evolution of spectral lines and the structure of the excited levels of Eu^{2+} in crystals of alkaline-earth fluorides(plastic deformation splitting and evolution of spectral lines and excited level structure of europium ion in alkaline-earth fluoride crystals),” *Optika I Spektroskopiia* **19**, 597–610 (1965).
- ³⁴C. Bungenstock, T. Tröster, and W. Holzapfel, “Effect of pressure on free-ion and crystal-field parameters of Pr^{3+} in $L\text{OCl}$ ($L = \text{La, Pr, Gd}$),” *Physical Review B* **62**, 7945 (2000).
- ³⁵F. Manjón, S. Jandl, K. Syassen, and J. Gesland, “Effect of pressure on crystal-field transitions of Nd-doped YLiF_4 ,” *Physical Review B* **64**, 235108 (2001).
- ³⁶T. Tröster and V. Lavin, “Crystal fields of Pr^{3+} in LiYF_4 under pressure,” *Journal of Luminescence* **101**, 243–251 (2003).
- ³⁷F. Manjón, S. Jandl, G. Riou, B. Ferrand, and K. Syassen, “Effect of pressure on crystal-field transitions of Nd-doped YVO_4 ,” *Physical Review B* **69**, 165121 (2004).
- ³⁸U. Rodríguez-Mendoza, A. Rodenas, D. Jaque, I. Martin, F. Lahoz, and V. Lavin, “High-pressure luminescence in Nd^{3+} -doped $\text{MgO}:\text{LiNbO}_3$,” *High Pressure Research* **26**, 341–344 (2006).
- ³⁹R. Turos-Matysiak, H. Zheng, J. Wang, W. Yen, R. Meltzer, T. Łukasiewicz, M. Świrkowicz, and M. Grinberg, “Pressure dependence of the $^3P_0 \rightarrow ^3H_4$ and $^1D_2 \rightarrow ^3H_4$ emission in $\text{Pr}^{3+}:\text{YAG}$,” *Journal of Luminescence* **122**, 322–324 (2007).
- ⁴⁰A. Kaminska, A. Kozanecki, M. Ramirez, L. Bausa, G. Boulon, M. Bettinelli, M. Boćkowski, and A. Suchocki, “Spectroscopic study of radiative intra-configurational $4f \rightarrow 4f$ transitions in Yb^{3+} -doped materials using high hydrostatic pressure,” *Journal of Luminescence* **169**, 507–515 (2016).
- ⁴¹R. M. Macfarlane, “Optical Stark spectroscopy of solids,” *Journal of Luminescence* **125**, 156–174 (2007).
- ⁴²R. Meltzer, H. Zheng, J. Wang, W. Yen, and M. Grinberg, “Pressure dependence of the $4f^15d^1 \rightarrow 4f^2$ emission of $\text{Pr}^{3+}:\text{YAG}$ using excited state absorption,” *Physica Status Solidi (c)* **2**, 284–288 (2005).

- ⁴³N. Ohlsson, M. Nilsson, S. Kröll, and R. Mohan, “Long-time-storage mechanism for Tm:YAG in a magnetic field,” *Optics Letters* **28**, 450–452 (2003).
- ⁴⁴F. de Seze, A. Louchet, V. Crozatier, I. Lorgeré, F. Bretenaker, J.-L. Le Gouët, O. Guillot-Noël, and P. Goldner, “Experimental tailoring of a three-level Λ system in Tm³⁺:YAG,” *Physical Review B* **73**, 085112 (2006).
- ⁴⁵Y. Sun, G. Wang, R. Cone, R. Equall, and M. Leask, “Symmetry considerations regarding light propagation and light polarization for coherent interactions with ions in crystals,” *Physical Review B* **62**, 15443 (2000).
- ⁴⁶R. L. Ahlefeldt, M. F. Pascual-Winter, A. Louchet-Chauvet, T. Chanelière, and J.-L. Le Gouët, “Optical measurement of heteronuclear cross-relaxation interactions in Tm:YAG,” *Physical Review B* **92**, 094305 (2015).
- ⁴⁷J. Bendat and A. Piersol, *Random data: analysis and measurement procedures* (John Wiley & Sons Inc., 1971).
- ⁴⁸R. Kalra, A. Laucht, J. P. Dehollain, D. Bar, S. Freer, S. Simmons, J. T. Muhonen, and A. Morello, “Vibration-induced electrical noise in a cryogen-free dilution refrigerator: Characterization, mitigation, and impact on qubit coherence,” *Review of Scientific Instruments* **87**, 073905 (2016).